Postbuckling mechanics of square slender steel plates in pure shear: Examining the role of second order effects

Maria E. Moreyra Garlock[1], Spencer E. Quiel[2], José Alós-Moya[3], Jonathan Glassman[4]

Abstract

Thin (slender) steel plates possess strength beyond the elastic buckling load which is commonly referred to as the postbuckling capacity. Semi-empirical equations based on experimental tests of plate girders have been used for decades to predict the ultimate postbuckling strength. However, several recent studies have shown that the current models for predicting the ultimate shear buckling capacity of thin plates are based on some incorrect assumptions of their mechanical behavior. As a result, the current design equations provide an approximate (albeit generally conservative) estimate of capacity based upon a range of test data parameters upon which they are founded. This paper explores the fundamental behavior of thin plates under pure shear. Such a fundamental examination of shear postbuckling behavior in thin plates is important because it will enable design procedures that can optimize a plate's shear strength and load-deformation performance for a wider range of loading and design parameters. Using finite element analyses (which are validated against available results of previous tests), outputs such as von Mises stresses, principal stresses, and principal stress directions are examined on both surfaces of a buckled plate acting in pure shear. The internal bending, shear, and axial stresses in the plate's finite elements are also evaluated. In this study, these evaluations are performed for a simply-supported plate with aspect ratio equal to 1.0 and slenderness equal to 134 - future work will examine a wider range of plate parameters. Results show that localized bending in the plates due to the out-of-plane postbuckling deformations appear to be a significant factor in the ultimate shear buckling capacity of the plate. Also, the compressive stresses continue to increase beyond elastic buckling in some regions of the plate, contrary to current design assumptions. Overall, this study provides new insights into the mechanics of shear postbuckling behavior of thin plates that can be exploited for improved design modifications compared to designs currently allowed in current practice.

1. Introduction

A significant portion of the bridge inventory in the US is supported with deep steel beams (e.g. plate girders) which have thin webs. The design of these elements is often controlled by the

---

[1] Associate Professor, Princeton University, <mgarlock@princeton.edu>
[2] Assistant Professor, Lehigh University, <seq213@lehigh.edu>
[3] Ph.D. Candidate, Universitat Politècnica de València, < joalmo11@gmail.com >
[4] Engineer, Exponent Failure Associates, <glassman.jonathan@gmail.com >

shear strength of that web plate. Web plates that elastically buckle due to shear load still possess a significant amount of *postbuckling* shear strength. Postbuckling capacity is utilized in the design of many bridge girders due to high web slenderness, which is necessitated by large girder depths and weight savings. This postbuckling behavior has attracted the attention of researchers and engineers since the 1880s. Since 1931, more than a dozen proposals have been developed to explain and predict the postbuckling shear strength of thin webs in plate girders; however, the true mechanics and postbuckling behavior is still not fully understood. Previous publications have provided extensive discussions on the various proposed plate shear buckling models throughout the literature (Ziemian, 2010; White & Barker, 2008; Yoo & Lee, 2006), and essentially all the models are based on *tension field action*. Tension field theory posits that the main source of this postbuckling shear strength is the development of tensile stresses in a defined diagonal field, which is mobilized after the onset of elastic shear buckling. Recent research, however, has shown that the fundamental assumptions upon which tension field action is based do not represent the full mechanical response of web-shear buckling (Yoo & Lee, 2006, Glassman & Garlock, 2016).

This paper explores the fundamental behavior of thin plates under pure shear. Using validated finite element analyses, outputs such as von Mises stresses, principal stresses, and principal stress directions are examined on both surfaces of the buckled plate. The internal bending, shear, and axial stresses in the plate elements are also evaluated. These evaluations are performed for a plate with aspect ratio equal to 1.0 and slenderness equal to 134. Future work will examine a wider range of plate parameters and potential design modifications.

2. Finite Element Model

The plate used for this study is based on standard plans for typical steel girder highway bridges specified by the Federal Highway Administration (FHWA). The 27.4-meter (90-foot) span design was used as a prototype, where the depth, D, equals 1473 mm, and the web thickness, t_w, equals 11 mm. In practice, many of these girders are designed with transverse stiffener spacing, a, greater than D; however, in this study, for simplification, we assume $a = D$. Future work will examine other stiffener spacings. The steel material is assumed to have a nominal yield stress of 345 MPa (50 ksi), which is common for many existing girders.

The finite element (FE) model was developed using the software Abaqus and meshed using S4 shell elements (doubly curved, general-purpose, finite membrane strains). Simply supported boundary conditions in the out-of-plane direction were used on all four sides. Fig. 1 shows that the in-plane translation is restrained along one edge, which provides the reaction to produce pure shear in conjunction with the load P applied along the opposite edge. Mesh convergence studies were conducted using an eigenvalue extraction analysis. The final mesh selected is shown in Fig. 1, and equal to 37 x 37 elements (approximately 40 mm square each). The finite element solution for the elastic shear buckling load, V_{cr}, equaled 1532 kN. This value has less than 1% error compared to a theoretical solution of 1526 kN, which is obtained from Eq. (1):

$$\tau_{cr} = k \frac{\pi^2 E}{12\left(1 - v^2\right)\left(D/t_w\right)^2} \tag{1}$$

In Eqn. (1), τ_{cr}, is the elastic shear buckling stress, E is Young's modulus, v is Poisson's ratio, D is the depth of the plate, t_w is the plate thickness, and k is the elastic shear buckling coefficient. The value of k is a function of the span-to-depth ratio (a/D) of the plate and the boundary conditions supplied to its edges (Timoshenko & Gere, 1961). For a plate with $a/D = 1$ and simply supported on all four edges, k equals 9.34. D/t_w is the slenderness ratio and indicates how susceptible the plate girder is to web shear buckling. The elastic critical shear buckling load, V_{cr}, is calculated by multiplying Eq. (1) by $D \cdot t_w$.

The modeling approach described above was further validated with experimental tests for various a/D and D/t_w ratios. Glassman and Garlock (2016) show that in comparison with 16 experiments, the FE models have very good correlation to the ultimate shear buckling capacity, V_u, of the plates: the FE models predicted V_u values to within about 10% of the published experimental values with one exception where the flange-to-web thickness ratio (t_f/t_w) was quite large compared to other tests.
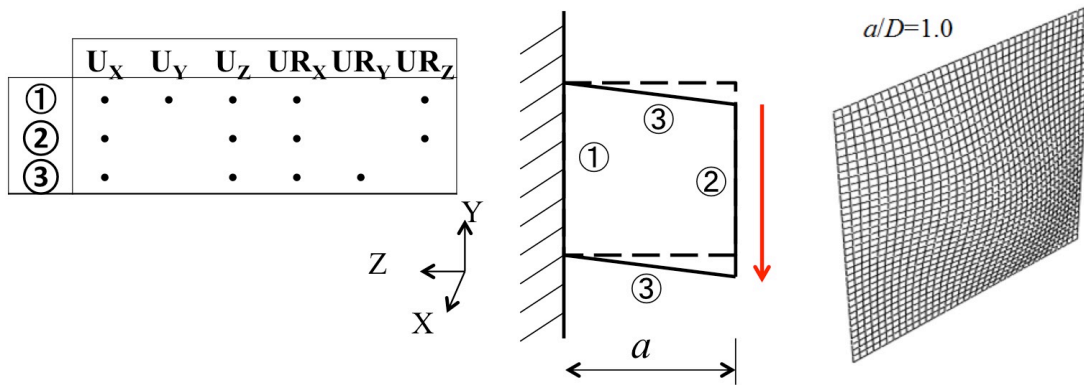

Figure 1: Boundary conditions of FE model (left), and mesh density in first mode buckled shape (right)

3. Results

3.1 Sign Conventions and Definitions

To properly interpret the finite elements results, the definitions and sign conventions of the stresses, moments, and rotations are clarified in the following list based on the Abaqus software:

- Tensile stresses are positive and compressive stresses are negative.
- SP:1 and SP:5 refer to the integrations points on the 'top' and 'bottom' surface of the plate, respectively (see Fig. 2).
- The element stresses, σ_1, σ_2, and σ_{12} are defined in Fig. 3a in the positive direction.
- Maximum principal stresses (σ_{max}) are the maximum positive value, thus typically corresponding to maximum tensile stresses. If no tension is present, the value will be negative, thus corresponding to the minimum compressive value. See Fig. 3b.
- Minimum principal stresses (σ_{min}) are the maximum negative value, thus typically corresponding to maximum compressive stresses. If no compression is present, the value will be positive, thus corresponding to the minimum tensile value. See Fig. 3b.
- Von Mises stresses are defined for the principal plane stress condition defined by Eq. (1), where σ_y is the yield stress. Fig. 4 plots this yield surface.

$$\sigma_y^2 = \sigma_1^2 + \sigma_2^2 - \sigma_1\sigma_2 \tag{1}$$
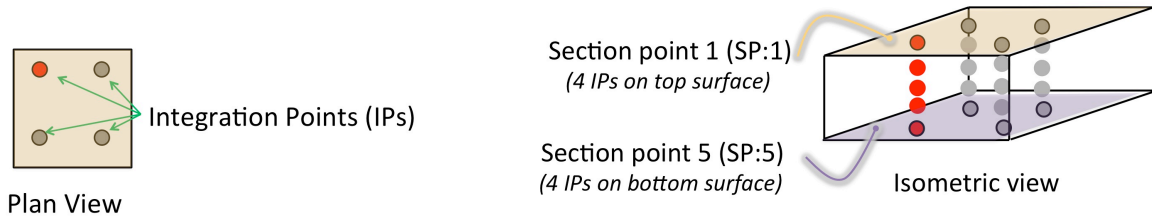
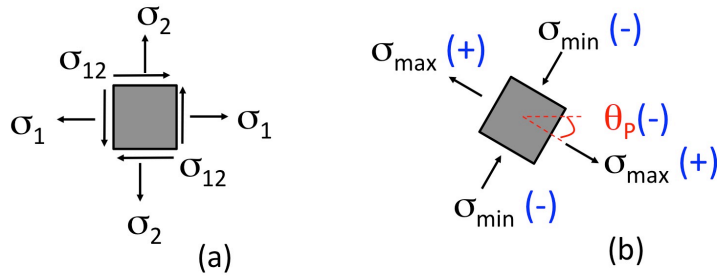Figure 2: Integration points and section points on the finite element

Figure 3: (a) Positive stresses on element; (b) Principal stresses and principal stress direction (with Abaqus sign convention in parenthesis).
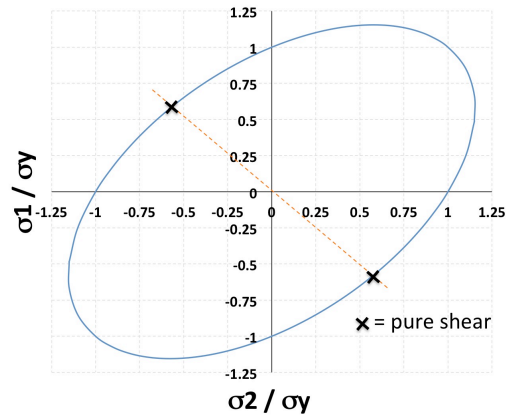

Figure 4: Von Mises yield surface

3.2 Ultimate Buckling Load, V_u, and Deformation

Fig. 5 illustrates the final deformed shape at the ultimate (postbuckling) shear load, V_u, which for this case study equaled 2634 kN. It can be seen that the out of plane deformations (U3) are represented in three half-wavelengths from Point B to Point D. The surface being shown in Fig. 5 represents the SP:5 face (see Fig. 2). Therefore, along the 'tension field' (from Point A to Point C, where the red color represents maximum positive U3), it will be shown that the SP:5 stresses will be in tension and SP:1 stresses will be in compression due to the significant bending in the plate. Conversely, in Fig. 5 where the deep blue shows large negative U3, SP:5 stresses will be in compression and SP:1 stresses will be in tension. A thorough analysis of the stresses will be discussed in sections to follow, where it will be shown that the plate bending due to this deformation dominates the response when V_u is reached.
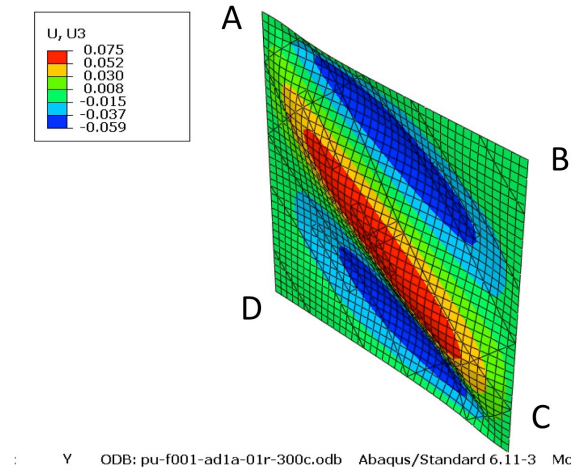
4

Figure 5: Deformed shape at V_u, with out of plane deformations, U3, shown in meters. The face shown (front face) corresponds to SP:5; the back face not shown corresponds to SP:1 (see Fig. 2).

3.3 Plate Behavior Just After Elastic Buckling

Before the plate reached elastic shear buckling, V_{cr}, the FE results were consistent with the theoretical behavior of a plate under pure shear: the angle of the principal stress, θ_p, was 45° and the principal stresses in tension and compression (σ_{max} and σ_{min}, respectively) were equal and opposite to one another and also equal to the shear stress ($V/(D \cdot t_w)$), where V is the applied load). Note that Abaqus does not output θ_p - this value was derived using σ_1, σ_2, and σ_{12} and the well-established equation based on Mohr's circle. In this section, the state of the plate when the shear V equals $1.15 \cdot V_{cr}$ (i.e. near the beginning of postbuckling behavior) is examined to enable a comparison to ultimate postbuckling behavior when V_u is reached.

- *Principal Stress Direction, θ_p:* Fig. 6 plots the θ_p contours for $V/V_u = 1.15$. It can be seen that this angle has not changed much from the pre-buckling state (before elastic buckling the angle was 45 degrees).
- *Principal Stresses:* Fig. 7 plots the σ_{min} and σ_{max} contours for $V/V_u = 1.15$. None of these stresses have reached yield and σ_{min} (compressive) is of comparable magnitude to σ_{max} (tension). At an elastic buckling load of 1532 KN, the elastic buckling stress theoretically equals 95 MPa. At $V = 1.15 V_{cr}$, Fig. 7 shows that both σ_{min} and σ_{max} have generally increased beyond 95 MPa.
- *von Mises Stresses*: Fig. 8 plots the von Mises stress contours for $V/V_u = 1.15$. The stresses are shown to be well below yield (= 345 MPa).

Though the contour patterns are similar, Figs. 6 through 8 all show some variation in the magnitudes of plotted results between the SP:1 and SP:5 faces of the plate. More significant levels of variation are shown for the principal and von Mises stresses in Figs. 7 and 8. These results highlight the emergence of bending moment through the thickness of the postbuckled plate in addition to in-plane stress. These moments are caused by second order bending due to compression of the buckled plate. Each of the three half wavelengths of this prototype's buckled shape experiences "bulging" as the top right and bottom left corners of the plate (see Fig. 5) are pushed closer together by the pure shear force.
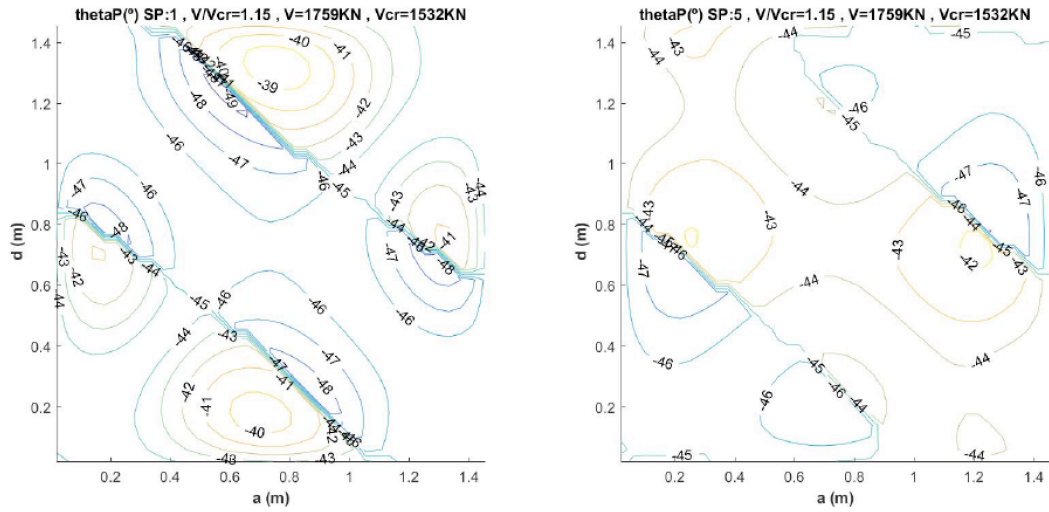
5

Figure 6: Principal Stress Direction, θ_p, for V/V_u = 1.15 in degrees. Left SP:1, Right SP:5 (See Figs. 2, 3).
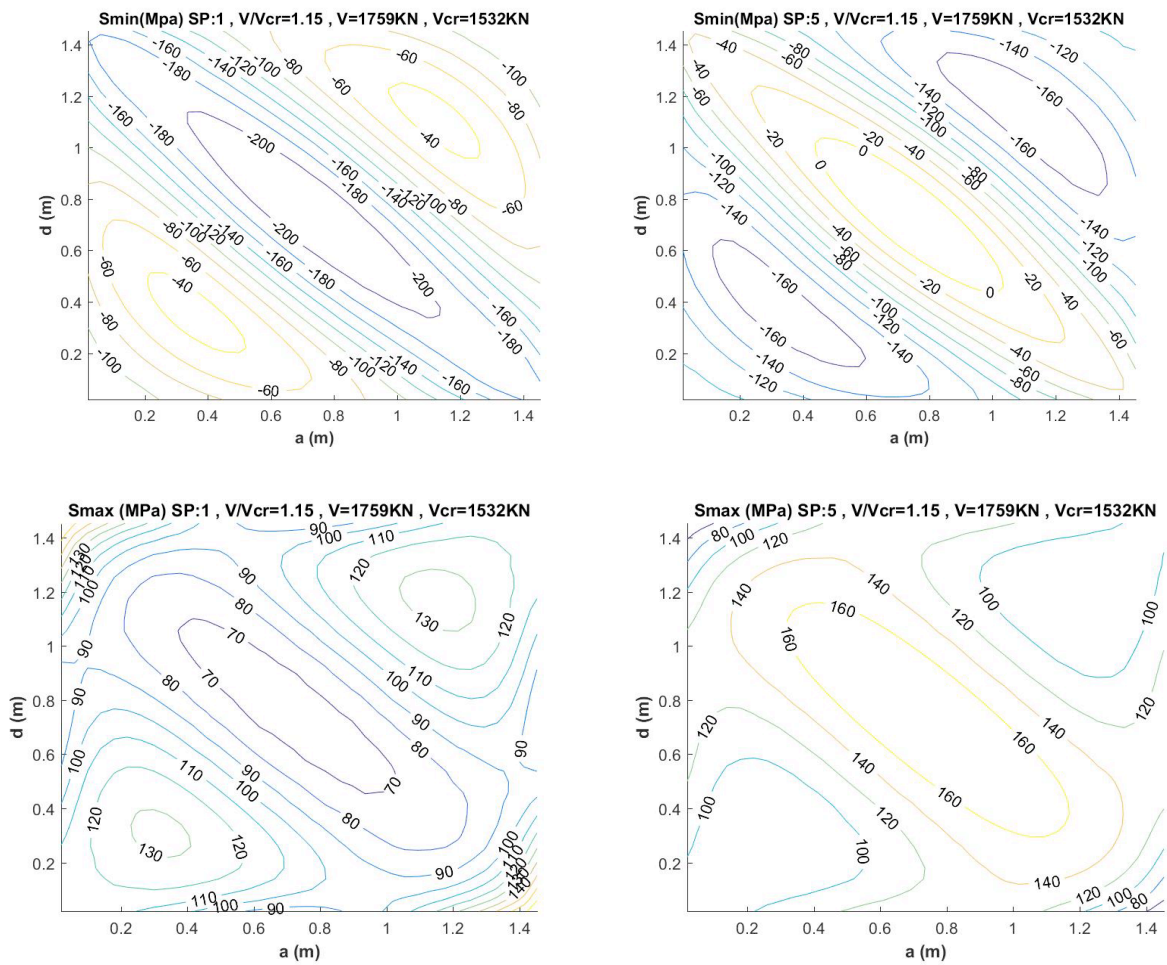

Figure 7: Principal Stresses, σ_{min} (top) and σ_{max} (bottom) for V/V_u = 1.15 (MPa). Left SP:1, Right SP:5 (See Figs. 2, 3).
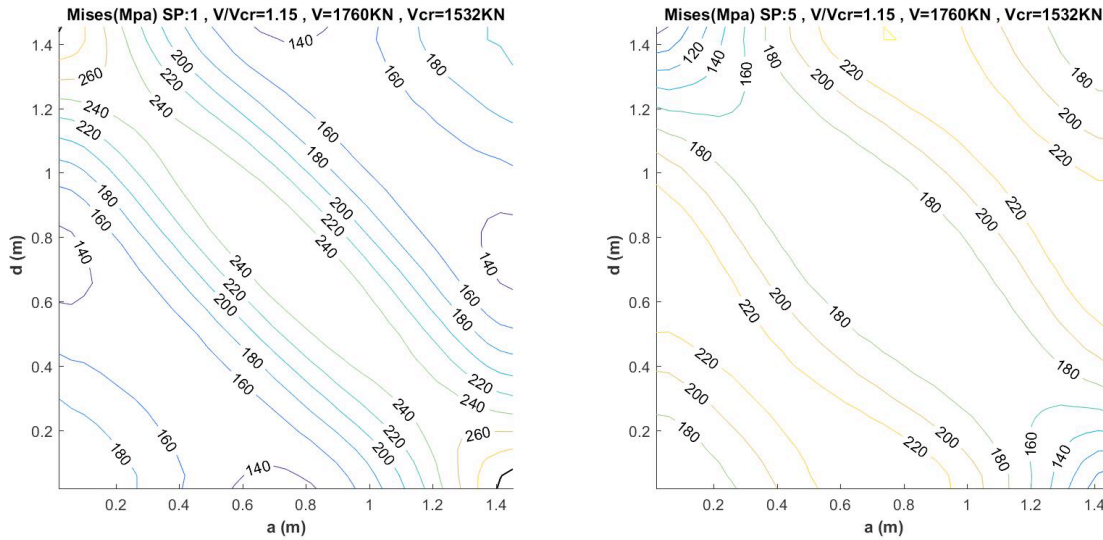
Figure 8: von Mises Stresses for V/V_u = 1.15 (MPa). Left SP:1, Right SP:5 (See Figs. 2, 3, 4).

3.3 Plate Behavior at the Ultimate Shear Buckling Load, V_u
In this section, we examine the stress state of the plate when the shear V equals the ultimate shear buckling load, V_u, which has a value of 2634 kN.

- *Principal Stress Direction, θ_p:* Fig. 9 plots the θ_p contours for $V = V_u$. It can be seen that this angle is no longer 45 degrees - it ranges between 20 and 50 degrees. Also, the values are now significantly different on each face (SP:1 and SP:5) since the principal stresses are different on each face. θ_p is shown to be largely dependent on the out-of-plane postbuckled deformation.

- *Principal Stresses:* Fig. 10 plots the σ_{min} and σ_{max} contours for $V = V_u$. σ_{max} has reached yield (as shown by the bold lines), and σ_{min} is close to yield. The magnitudes and signs (positive, negative) are related to the deformation (and bending) of the plate at V_u as seen in Fig. 5. The σ_{max} contours for SP:5 in Fig. 10 show a distinct band of yielding in the tension field direction, which generally supports the assumptions in the current state of practice. However, the corresponding plot for SP:1 shows much lower maximum stress (actually remaining negative) in this same region due to bending. The maximum stresses at yield for SP:1 are instead located along two smaller bands that are parallel to the tension field direction but located about half the perpendicularly distance from the tension diagonal to each corner. The σ_{min} contour for SP:1 shows near-yield compressive stresses (~300 MPa) along the tension field direction. These stresses represent the compression face of bending in the buckled half-wavelength along the diagonal. The emergence of these large compressive stresses on the SP:1 face indicates that the large tensile stresses in the tension field on the SP:5 face are cause by a combination of in-plane stress and second-order bending.
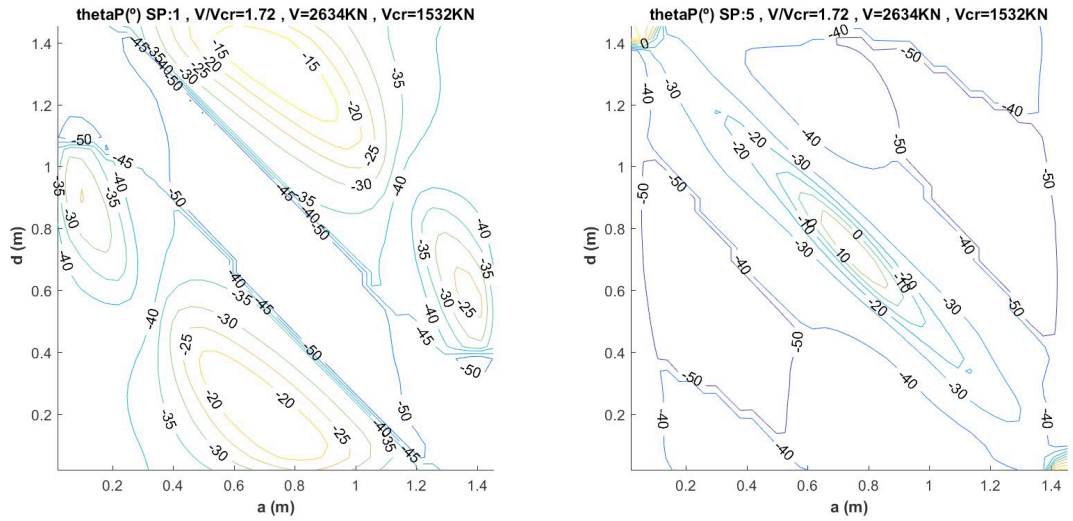
7

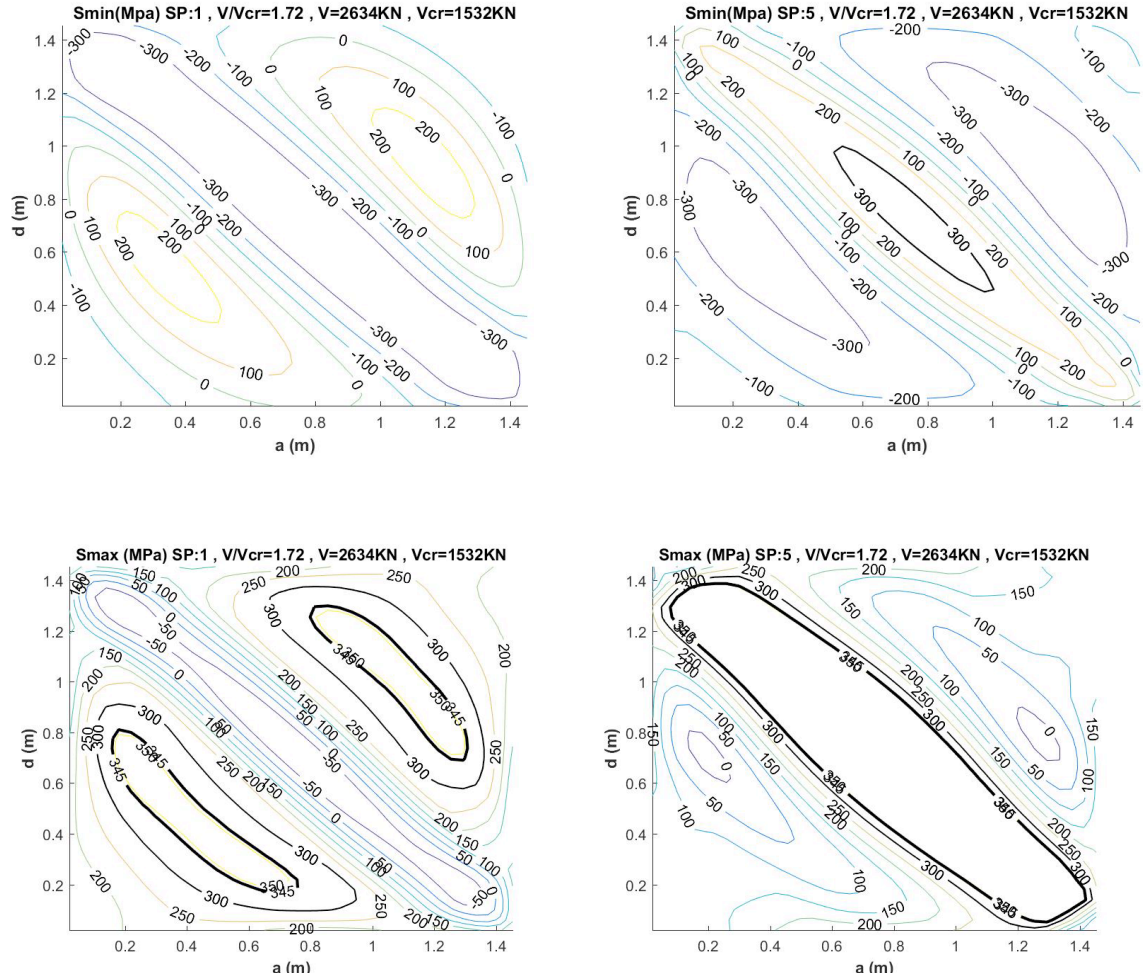Figure 9: Principal Stress Direction, θ_p, for $V = V_u$ in degrees. Left SP:1, Right SP:5 (See Figs. 2, 3).

Figure 10: Principal Stresses, σ_{min} (top) and σ_{max} (bottom) for $V = V_u$ (MPa). Left SP:1, Right SP:5 (See Figs. 2, 3).

- *von Mises Stresses*: Fig. 11 plots the von Mises stress contours for $V = V_u$. The stresses on almost all of the plate surface have reached yield (at 345 MPa, again shown with bold lines) on both faces. At ultimate shear, the plate experiences a saturation of von Mises yielding due to the combination of internal forces that develops in its buckled shape. Fig. 11 shows that face SP:5 experiences a more widespread saturation of von Mises yielding than SP:1, which has a distinct band of yielding along the tension field diagonal. Note that bending-induced compression stress has caused von Mises yielding in the tension field diagonal on face SP:1 rather than in-plane tensile stresses. This deviates from the current state of practice which assumes in-plane stress to be the primary contributor to reaching ultimate shear capacity.
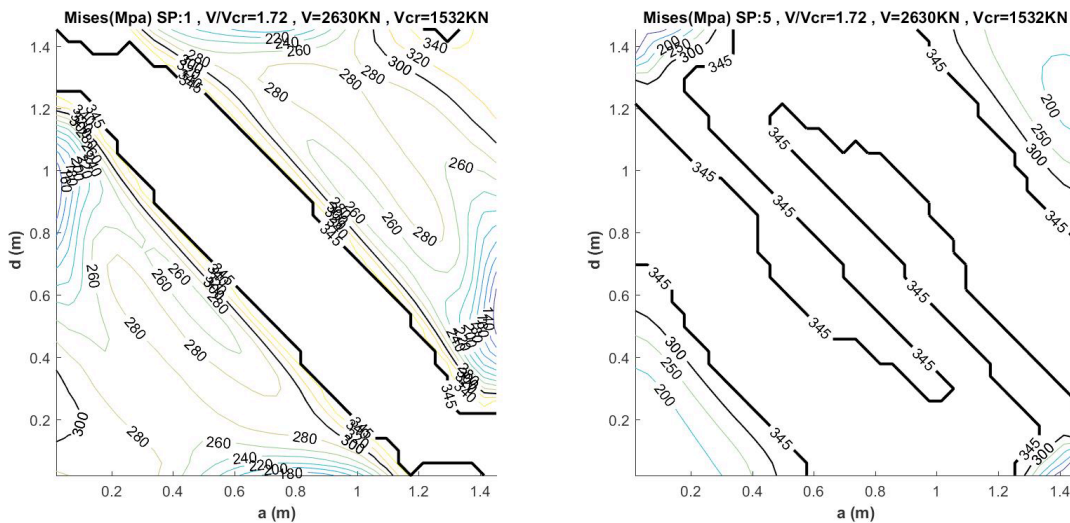

Figure 11: von Mises Stresses for $V = V_u$ (MPa). Left SP:1, Right SP:5 (See Figs. 2, 4).

3.4 Bending Stresses at the Ultimate Shear Buckling Load, V_u

The results presented thus far indicate that bending through the thickness of the plate due to postbuckling out-of-plane deformations has a large effect on the stress distribution. In this section, the axial stress is separated from the bending stress for both σ_1 and σ_2 (see Fig. 3). The axial stress is the average of the stress on SP:1 and SP:5. Assuming that the plane section through the plate's thickness remains plane, the bending stress through that thickness is approximated as the stress on SP:1 minus the stress on SP:5, divided by two. Fig. 12 presents the results for both σ_1 and σ_2. It is clearly seen that bending stresses dominate. Bending stress is on the order of 2 times larger than axial stress for σ_1 and similarly on the order of 10 times larger for σ_2. These plots clearly show that second-order moment in the postbuckled shape makes a significant contribution to the onset of ultimate shear capacity.
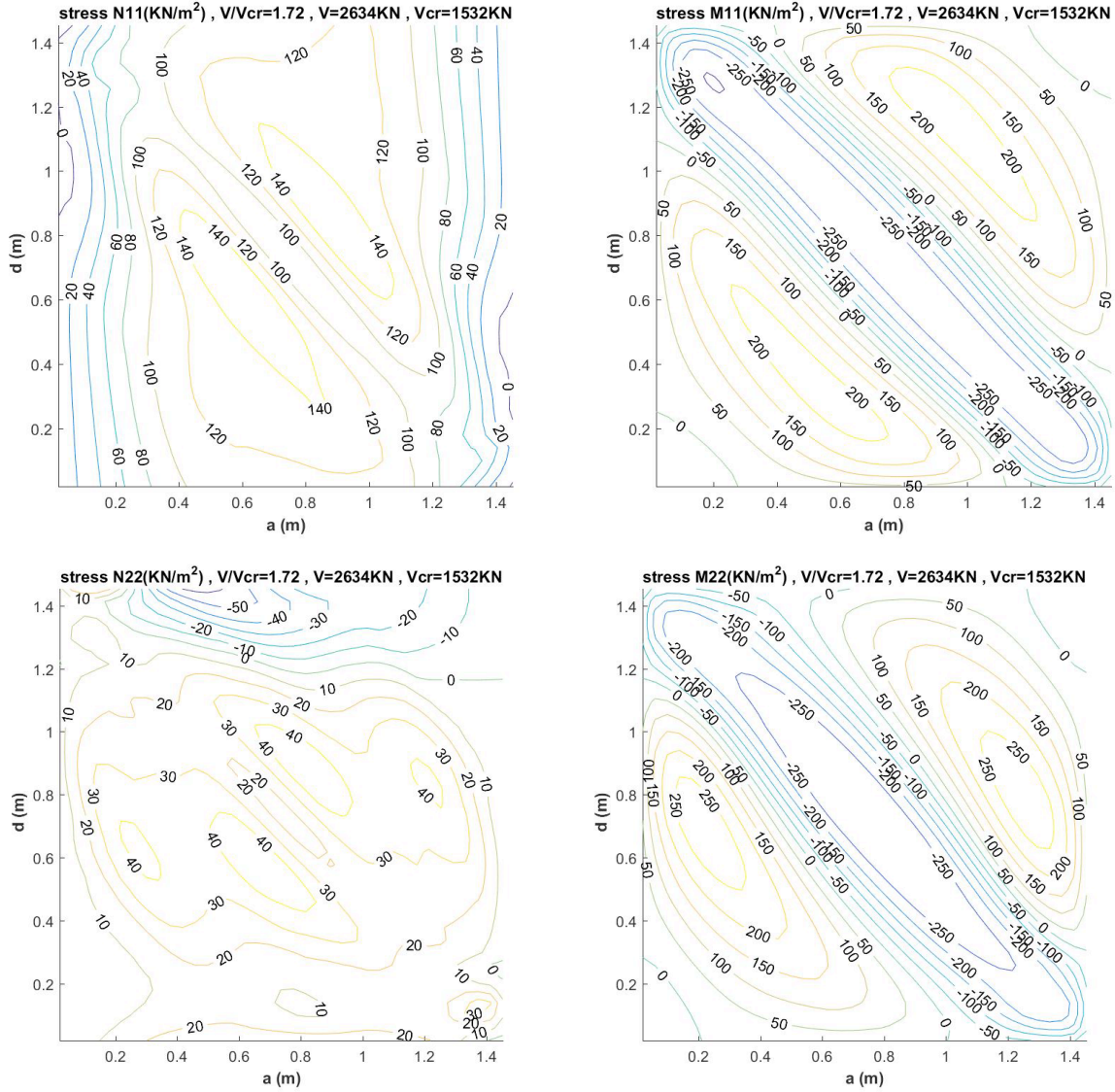
9

Figure 12: Axial stresses (left) and bending stresses (right) for $V = V_u$ (MPa). Top figures are for σ_1 and bottom are for σ_2. See Fig. 3.

Fig. 13 provides additional illustration of the bending in the plate. It plots σ_{min} and σ_{max} for the element in the center of the plate on both surfaces SP:1 and SP:2. These stresses are plotted against the analysis increment number until V_u is reached (increment 1693). By zooming in on the first 350 increments of the analysis in Fig. 13, one clearly observes the point of elastic shear buckling where SP:1 and SP:5 diverge at increment 313. This increasing divergence clearly indicates the onset of second order bending moment through the thickness of the plate. At V_u, SP:1 and SP:5 are significantly different for both σ_{min} and σ_{max}.
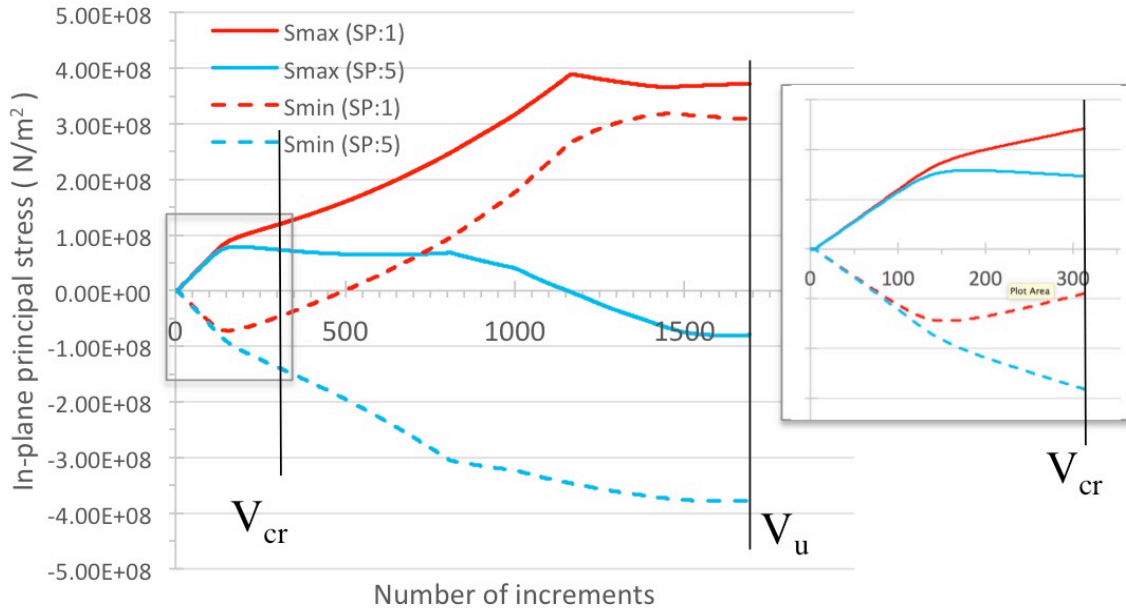
Figure 13: σ_{min} (Smin) and σ_{max} (Smax) for the element in the center of the plate on both surfaces SP:1 and SP:5. Elastic shear buckling occurs at increment 313, and ultimate shear buckling occurs at increment 1693.

4. Reducing the Compressive Response

The results presented in Section 3 indicate that compression and second order bending stresses (due to large out-of-plane deformations) play an important role in the postbuckling performance of this slender plate. A strategy to reduce compression and out-of-plane deformations would be to interrupt the continuity of the compression field (i.e. in the diagonal direction opposite the tension field), thereby reducing the severity of postbuckling compression-driven deformation. To this end, the plate was modified in two ways: (1) by cutting the compression field corners by 16% of the depth D (model name = CUT), thus reducing the area by 3%; and (2) by cutting slits near the corners along the compression field (model name = SLITS), thus reducing the area by 1%. Images of these models and the resulting V_{cr} and V_u values obtained from finite element analysis are shown in Table 1. Contour plots of the von Mises stress when the plate reaches V_u are shown for each case in Fig. 14.

As would be expected, Table 1 shows that interrupting the compression field will delay the onset of elastic buckling and increases V_{cr} by at least 14%. For the CUT case, V_u is unaffected since the cut corners do not deter the development of similar von Mises stress patterns as the FULL original plate, as shown in Fig. 14. For the SLITS case, V_u is slightly reduced but still produces similar von Mises yield stress saturation at ultimate shear capacity as the other cases. These results suggest that the elastic buckling load could be strategically modified to meet a given design objective with relatively minor modification to the plate. The mechanical impact and construction/life-cycle implications of these modifications will be examined in future research by the authors.

11

Table 1: Finite element results of modified plates.

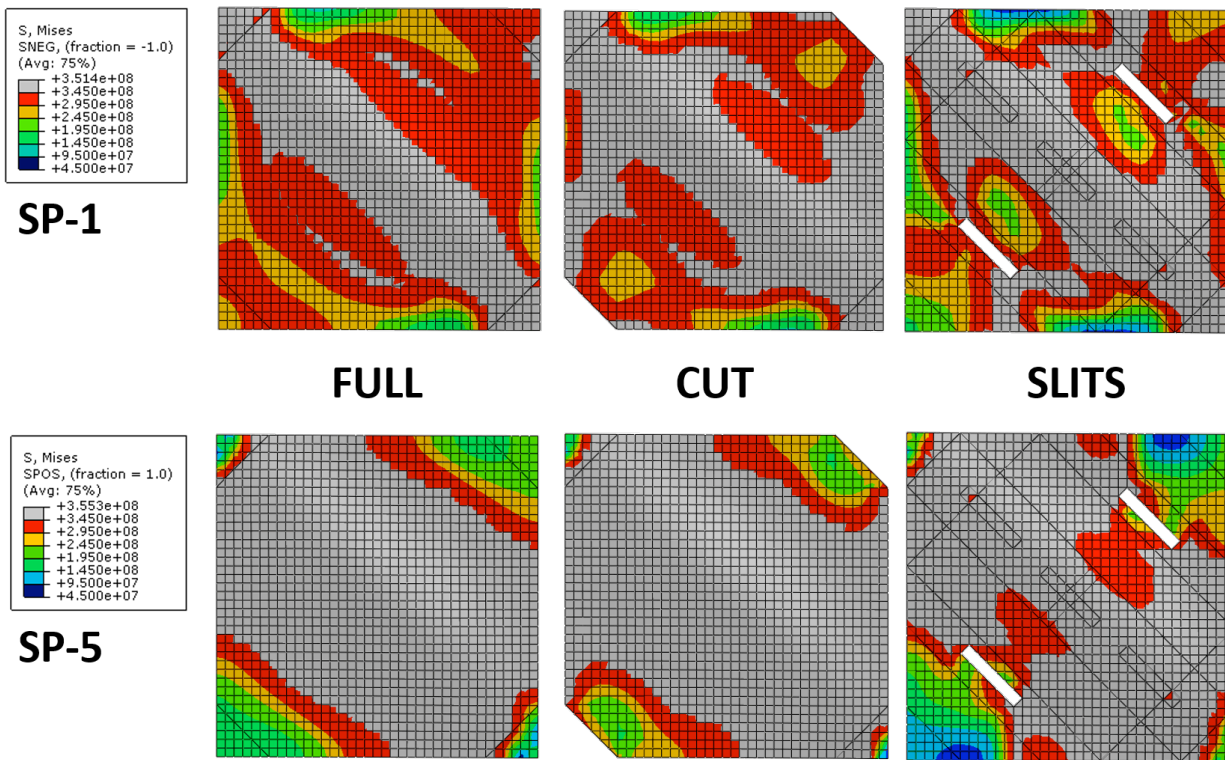|		Vcr (KN)	Vu (KN)
		(ratio to baseline)	
FULL (baseline)		1532 (1.0)	2640 (1.0)
CUT		1838 (1.20)	2640 (1.0)
SLITS		1745 (1.14)	2516 (0.95)

Figure 14: von Mises stresses at V_u for the FULL plate, the CUT plate, and the plate with SLITS (units = Pa).

4. Summary and Conclusions

Postbuckling behavior of slender webs in steel plate girders has been a mainstay of bridge design for several decades on the basis of semi-empirical equations that were originally developed in the 1960's. Though the existing state of practice is generally conservative, the assumption of pure in-plane stress in response to shear loads after the web has buckled does not capture the full mechanical performance of the thin plate. New research by the authors has begun to reexamine the postbuckling behavior of thin steel plates by considering the combined effects of in-plane stress and out-of-plane bending. This study utilized previously validated finite element models to analyze a prototype simply supported plate with an aspect ratio equal to 1.0. The results of these analyses showed that the out-of-plane bulges of the postbuckled plate develop second order

moments due to compression along the diagonal opposite the tension field. Some conclusions from this initial study include the following:

- At the ultimate shear buckling load, V_u, the angle of principal stress direction is no longer 45 degrees - it ranges between 20 and 50 degrees.
- The stress distribution through the plate thickness was separated into pure planar (i.e. axial) and bending stresses. Bending stresses were found to be significantly higher than the pure planar stresses at the ultimate shear buckling load. These stresses are created by second order compression of the plate's buckled shape (i.e. the buckled half-wavelengths essentially create "springs" along the length of the compression field diagonal).
- At the ultimate shear buckling load, almost the entire plate has reached the von Mises yield boundary due to a combination of planar and bending stress. The contours of von Mises yielding show some differences, however, for the opposing faces of the plate.
- The compression diagonal continues to offer resistance to shear following buckling; again, this is mostly due to second order bending of the buckled shape.

Building off this result, the authors examined some simple modifications of the plate which would alter the compression-driven postbuckling moment behavior by interrupting the compression diagonal. The results of two cases, with small through-plate cuts removed from the compression diagonal, showed (1) an increase of at least 14% in the shear load needed to induce buckling (i.e. elastic shear buckling load) and (2) a negligible effect on the ultimate shear buckling load. These results indicate that the onset of elastic buckling can be delayed by interrupting the compression field, which may prove useful for designing girder webs.

References
Glassman, J., and Garlock, M. (2016). "A Compression Model for Ultimate Postbuckling Shear Strength". *Thin-Walled Structures*, vol. 102, pp. 258–272.
Timoshenko, S. P. and Gere, J. M. (1961). *Theory of Elastic Stability*, Second Edition, New York: McGraw-Hill Book Company, Inc.
White D. W. and Barker M. G. (2008) "Shear Resistance of Transversely Stiffened Steel I-Girders," *Journal of Structural Engineering*, vol. 134, no. 9, pp. 1425-1436.
Yoo, C. H. and Lee, S. C. (2006). "Mechanics of Web Panel Postbuckling Behavior in Shear," *Journal of Structural Engineering*, vol. 132, no. 1, pp. 1580-1589.
Ziemian, R. D. (2010). *Guide to Stability Design Criteria for Metal Structures*, 6th ed., Hoboken: John Wiley & Sons.